

RESEARCH ARTICLE

Aggregation-induced emission enhancement of anthracene-derived Schiff base compounds and their application as a sensor for bovine serum albumin and optical cell imaging

Simon Densil¹ | Chien-Huei Chang² | Chia-Ling Chen² | Alagarsamy Mathavan¹ | Arumugam Ramdass³ | Veerasamy Sathish⁴ | Pounraj Thanasekaran² | Wen-Shan Li² | Seenivasan Rajagopal⁵

¹Department of Chemistry, V. O. Chidambaram College, Thoothukudi, India

²Institute of Chemistry, Academia Sinica, Taipei, Taiwan

³Department of Chemistry, Aditanar College of Arts and Science, Tiruchendur, India

⁴Department of Chemistry, Bannari Amman Institute of Technology, Sathyamangalam, India

⁵Postgraduate and Research Department of Chemistry, Vivekananda College, Tiruvudagam West - 625 234, Madurai, India

Correspondence

S. Rajagopal, Postgraduate and Research Department of Chemistry, Vivekananda College, Tiruvudagam West - 625 234, Madurai, India.
Email: rajagopalseenivasan@yahoo.com

W.-S. Li, and P. Thanasekaran, Institute of Chemistry, Academia Sinica, Taipei, 115 Taiwan.

Email: wenshan@gate.sinica.edu.tw; ptsekaran@yahoo.com

Funding information

Department of Science and Technology, Ministry of Science and Technology; Ministry of Science and Technology; Academia Sinica and the National Science Council, Grant/Award Numbers: MOST 103-2113-M-001-024-MY3 and NSC 102-2325-B-001-025; SERB-Indo US; UGC-BSR Faculty Fellowship and Emeritus Fellowship

Abstract

Three anthracene-based Schiff base complexes, **R1–R3** (**R1** = (E)-N'-((anthracen-10-yl)methylene)benzohydrazide; **R2** = (E)-1-((anthracen-10-yl)methylene)-4-phenylsemicarbazide; and **R3** = (E)-1-((anthracen-10-yl)methylene)-4-phenylthiosemicarbazide) were synthesized from 9-anthracenecarboxaldehyde, benzohydrazide, 4-phenylsemicarbazide and 4-phenylthiosemicarbazide respectively, and characterized by various spectral techniques. The absorption spectral characteristics of **R1–R3** were bathochromically tuned to the visible region by extending the π conjugation. These target compounds were weakly fluorescent in tetrahydrofuran (THF) solution because of rapid isomerization of the C=N double bond in the excited state. However, the aqueous dispersion of **R1–R3** in the THF/water mixture by the gradual addition of water up to 90% resulted in an increase in the fluorescence intensity mainly due to aggregation-induced emission enhancement (AIEE) properties. The formation of nanoaggregates of **R1–R3** were confirmed by scanning electron microscopy (SEM) and atomic force microscopy (AFM) techniques. The compounds **R1–R3** are ideal probes for the fluorescence sensing of bovine serum albumin (BSA) and breast cancer cells by optical cell imaging.

KEYWORDS

aggregation-induced emission enhancement, anthracene-based Schiff base, biosensor, BSA, C=N isomerization, optical imaging

Abbreviations used: ACQ, aggregation-caused quenching; AIE, aggregation-induced emission; AIEE, aggregation-induced emission enhancement; AFM, atomic force microscopy; BSA, bovine serum albumin; DMEM, Dulbecco's modified Eagle's medium; DMSO, dimethyl sulphoxide; EDX, energy dispersive X-ray; HPLC, high pressure liquid chromatography; HSA, human serum albumin; IR, infra-red; NMR, nuclear magnetic resonance; PBS, phosphate-buffered saline; SEM, scanning electron microscopy; THF, tetrahydrofuran; TPE, two-photon excitation; UV, ultraviolet.

1 | INTRODUCTION

There has been an increasing upsurge over the past 2 decades in interest in fluorescent materials due to their various application in organic light-emitting devices and in the biological and materials sciences.^[1–4] Researchers strive to improve the quantum efficiency of fluorescence of organic molecules because most organic materials are non-luminescent or weakly luminescent in the aggregation or solid state due to the aggregation-caused quenching (ACQ) effect, problematic for common

organic chromophores.^[5] This notorious ACQ phenomenon greatly limits the real-world application of organic fluorophores in the solid state.^[6]

To completely eradicate the ACQ effect, a unique phenomenon called 'aggregation-induced emission' (AIE) was coined by Tang and co-workers in 2001 using siloles.^[7,8] When a molecule is non-luminescent in the dissolved state but strongly fluorescent in the aggregated state through restriction of free intramolecular rotation of the molecule, it is said to have AIE characteristics. This fluorescence enhancement is due to the prohibition of energy dissipation via non-radiative channels.^[9] Conversely, if the emission of a weakly luminescent chromophoric material is enhanced by aggregate formation the phenomenon is called aggregation-induced emission enhancement (AIEE).^[10] Over the past decade, many research groups have enthusiastically worked on the design of new AIE/AIEE molecules, on manipulation of their mechanism and on morphological structures for their application.^[11-13] We wish to record here that we report the first AIEE effect observed in metal complexes.^[14,15] To date, a plethora of AIE/AIEE active organic compounds have been reported viz. siloles,^[16] tetraphenylethene derivatives^[17,18], maleimide^[19], crown-ether^[20], stilbene derivatives^[21], 1-cyano-trans-1,2-bis-(4'-methylbiphenyl)ethylene (CN-MBE)^[22,23], quinoline derivatives^[24], pyrazole derivatives^[25,26], and organic borane compounds etc.^[27,28] Organic fluorophores with AIE/AIEE characteristics have received enormous interest due to their potential application for detection of biomolecules, especially with high selectivity and sensitivity for molecular sensing and detection of insulin fibrils, responsible for diabetes.^[29] In bioimaging application studies, AIEE materials showed intriguing benefits including low photodamage, deep tissue penetration and minimal autofluorescence.^[30] Here, we report our results on an application for sensing and imaging biological compounds based on AIEE probes. The rationale for AIE/AIEE is supported by various mechanisms such as restriction of intramolecular rotation (RIR)^[31], photo-induced electron transfer (PET)^[32], J-aggregate formation^[33], twisted intramolecular charge transfer (TICT)^[34], aggregation of long alkyl chains^[35] and *trans-cis* isomerization.^[36] Among these different mechanisms, restriction due to C=N conformation rotation has greatly limited their use.^[37,38]

Serum albumins are important proteins in blood plasma that are synthesized by the parenchymal cells of the liver.^[39] Bovine serum albumin (BSA) is used as a model compound for biological studies due to its medical importance, low cost, easy availability, intrinsic fluorescence emission, and 76% structural similarity with human serum albumin (HSA).^[40] It is a heart-shaped protein containing a single polypeptide chain that consists of 583 amino acid residues with 17 disulfide bonds and one free SH group with a molecular weight of 66 kDa. The tertiary structure of BSA consists of three domains (I, II and III) and each domain contains two sub-domains (A and B).^[41] BSA fluorescence is due to tryptophan (Trp) residues at positions 134 and 212 of the amino acid sequence. It is responsible for the transport, distribution and deposition of various endogenous and exogenous substances in our body.^[42] Hence, it is worth investigating the interaction between this protein and fluorescent compounds because drugs are transported in the blood bound to albumin.^[43] Anthracene-based derivatives are used as fluorescent probes to study binding to

biological molecules.^[44] They are employed in the treatment of metastatic breast cancer, acute lymphoblastic leukaemia, non-Hodgkin's lymphoma, and metastatic prostate cancer.^[45] The use of anthracene-containing compounds such as chemotherapeutic agents has been explored and demonstrated in clinical trials.^[46]

With this background and the unique behaviour of the anthracene moiety in connection with biological molecules, we have designed simple but highly effective receptors, i.e. amide, urea and thiourea moieties of Schiff base derivatives. Among the reported AIE/AIEE compounds, Schiff base compounds are the ideal compounds to explore AIEE because they have C=N isomerization moiety and conjugated double-bond terminated fluorophores.^[47] Attaching Schiff base derivatives to organic or metal units to serve as optical sensors is a good approach for study.^[48,49] Only a few reports on anthracene derivatives are available, and these show high fluorescence efficiency in their solid states and the AIE/AIEE phenomenon.^[50-56] In addition, efforts have been made to design organic fluorophores coupled with the dynamic interactions of biologically important species that can be visualized by fluorescence microscopy.^[57] However, anthracene compounds with AIEE behaviour and used in biosensor and cellular imaging studies have not been reported so far. Through the introduction of optical and biological functionality of anthracene chromophores, the aim of the present study was to investigate the AIEE characteristics of anthracene-based derivatives **R1-R3** with a view to exploiting their potential application as sensors for BSA and in optical cell imaging studies in cancer cells.

2 | EXPERIMENTAL

2.1 | Materials

Benzohydrazide, 4-phenylsemicarbazide, 9-anthracenecarboxaldehyde and 4-phenylthiosemicarbazide were procured from Sigma-Aldrich. All other chemicals were obtained from commercial sources and used as received.

2.2 | Instrumentation

The electronic absorption spectra were recorded on a JASCO variant 630 spectrophotometer using 1 cm path length cuvette. Emission spectra were measured using a JASCO FP 8300 spectrofluorometer. In order to measure the emission spectrum in the solid state, film samples were prepared by drop casting and subsequent spin-coating from tetrahydrofuran (THF) solutions (100 ml) onto a quartz cell. Infra-red spectra were recorded on a Perkin-Elmer Fourier transform infra-red (FT-IR) spectrometer PARAGON 1000, and ¹H nuclear magnetic resonance (NMR) spectra on a Bruker 300 MHz NMR spectrometer. FAB-MS data were obtained using a JEOL, JMS-700 double focusing mass spectrometer. The morphology of the nanoaggregates was studied using scanning electron microscopy (SEM) (Carl Zeiss) equipped with energy dispersive X-ray analysis (EDX). The atomic force microscopy (AFM) image was obtained on a PicoPlus AFM instrument (Molecular Imaging Inc., Arizona, USA) operating in the noncontact mode. AFM images were taken under dry conditions. An NCL cantilever was used to scan the sample at a frequency of 177 kHz and a scanning speed

2.4 lines/s. Stock solutions for compounds **R1–R3** (1×10^{-3} M) were prepared in aqueous THF for BSA binding studies. For binding studies with biomolecules, complexes **R1–R3** were dissolved in 2% THF:98% water (v/v). The sample solution containing BSA (1×10^{-3} M) was prepared using phosphate-buffered saline (PBS) buffer (pH 7.4). The PBS buffer solution was prepared using a mixture of disodium hydrogen phosphate, sodium dihydrogen phosphate and sodium chloride at pH 7.4. Freshly prepared sample solutions were used for each measurement. High pressure liquid chromatography (HPLC) grade THF and double-distilled water were used in all photophysical and photochemical measurements. Emission quantum yield was measured using a quinine sulfate in 0.1 N H_2SO_4 as a standard solution.^[58]

2.3 | General procedure for the preparation of anthracene-based compounds, R1–R3

The anthracene-based receptors **R1–R3** were obtained by thoroughly mixing an ethanolic solution of 9-anthracenecarboxaldehyde (2.42 mmol) and the corresponding amines (2.67 mmol) (Scheme 1). A few drops of acetic acid were added and the mixture refluxed at 75–80°C for 3 h. After the reaction, anthracene derivatives **R1–R3** were obtained as golden yellow solids. The reaction mixture was filtered hot, washed with hot ethanol, and dried under vacuum to obtain a desired product. The yield of the products **R1–R3** ranged from 91 to 94%. The prepared compounds were characterized by various spectral techniques (Figures S1–S7).

2.3.1 | Characterization of (E)-N'-(anthracen-10-yl)methylene)benzohydrazide (R1)

Yield: 94%; m.p.: 202°C; IR (KBr, cm^{-1}) ν : (C=N) 1649, (N-H) 3200 and 3055, (C=O) 1545; $^1\text{H-NMR}$ (300 MHz, CDCl_3) δ H: 7.21–8.43 (ArH), 8.53 (s, 1H, C-H), 9.23 (s, 1H, N-H); ESI-MS (m/z): calcd. for $\text{C}_{22}\text{H}_{15}\text{N}_2\text{O}$ [M-H⁺]: 324.4; found: 323.1; Elemental analysis for $\text{C}_{22}\text{H}_{15}\text{N}_2\text{O}$: calcd. C, 81.38%; H, 4.62%; N, 8.63%; O, 4.93%; found: C, 81.71%; H, 4.64%; N, 8.67%; O, 4.95%.

2.3.2 | Characterization of (E)-1-((anthracen-10-yl)methylene)-4-phenylsemicarbazide (R2)

yield: 93%; m.p.: 212°C; IR (KBr, cm^{-1}) ν : (C=N) 1690, (N-H) 3390, (C=O) 1540; $^1\text{H-NMR}$ (300 MHz, CDCl_3) δ H: 7.06–8.46 (ArH), 8.90 (s, 1H, C-H), 9.13 (s, 1H, N-H), 10.31 (s, 1H, N-H). ESI-MS (m/z): for $\text{C}_{22}\text{H}_{17}\text{N}_3\text{O}$ [M-H⁺]: calcd. 339.4, found: 338.2; Elemental analysis for $\text{C}_{22}\text{H}_{17}\text{N}_3\text{O}$: calcd. C, 77.78%; H, 5.01%; N, 12.37%; O, 4.71%; found: C, 78.06%; H, 5.03%; N, 12.41%; O, 4.73%.

2.3.3 | Characterization of (E)-1-((anthracen-10-yl)methylene)-4-phenylthiosemicarbazide (R3)

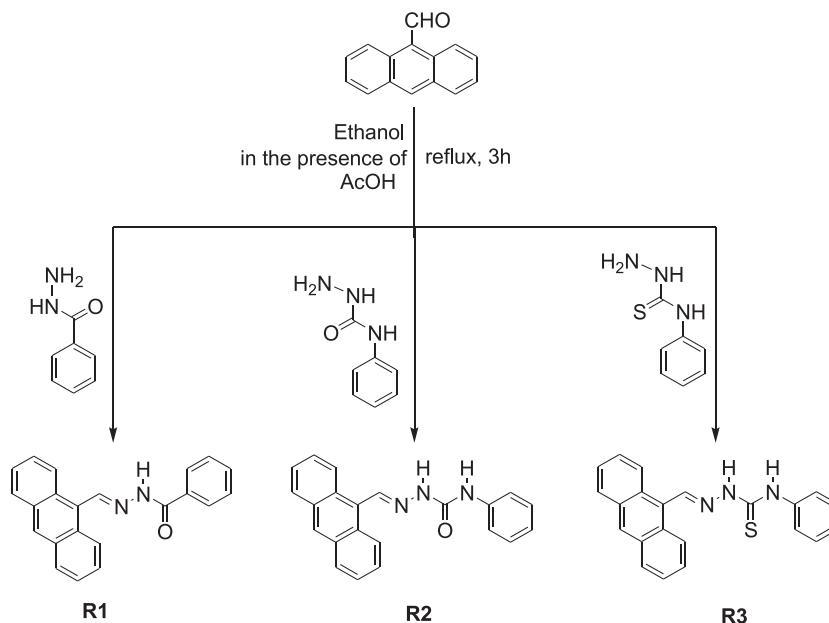
yield: 91%; m.p. 208°C; IR (KBr, cm^{-1}) ν : (C=N) 1607, (N-H) 3148 and 3330; $^1\text{H NMR}$ (400 MHz, CDCl_3) δ H: 7.155–8.611 (Ar-H), 8.732 (s, 1H, C-H), 10.022 (s, 1H, N-H), 12.073 (s, 1H, N-H). ESI-MS (m/z): for $\text{C}_{22}\text{H}_{18}\text{N}_3\text{S}$ [M-H⁺]: calcd. 355.5, found: 354.1; Elemental analysis for $\text{C}_{22}\text{H}_{18}\text{N}_3\text{S}$: calcd. C, 74.26%; H, 5.06%; N, 11.81%; S, 9.00%; found: C, 74.56%; H, 5.08%; N, 11.86%; S, 9.04%.

2.4 | Cell culture

BT-549 breast cancer cells (ATCC) were grown adherently and maintained in RPMI 1640 medium (GIBCO) containing 10% fetal bovine serum (FBS) and 0.023 IU/ml insulin. MDA-MB231 cells (ATCC) were maintained in Dulbecco's modified Eagle's medium (DMEM) medium (GIBCO) containing 10% FBS. All media contained 100 U per ml penicillin and 100 U per ml streptomycin.

2.5 | MTT cell viability assay

BT549 and MDA-MB231 were placed in 96 well plates and incubated at 37°C overnight. The cultured cells were treated with gradient concentrations of **R2** (final concentrations: 0, 10, 20, 30, 40, 50 μM) for 24 h, and viable cells were measured using an MTT (3-(4,5-dimethylthiazol-2-yl)-2,5-diphenyltetrazolium bromide) assay (Sigma). Cells were incubated with 100 μl MTT solution (1 mg/ml) for 4 h at 37°C, then the medium containing non-metabolized



SCHEME 1 Synthetic route for the preparation of anthracene-based receptor compounds, **R1–R3**

MTT was aspirated. Formazan crystals were dissolved in 100 μl dimethyl sulphoxide (DMSO), and absorbance was measured at 540 nm.

2.6 | Fluorescence detection of probes in living cells

Breast cancer cells (3×10^4 cells/well, BT549 and MDA-MB231 cells) were seeded on chambered cover glass (Thermo Scientific™) and incubated at 37°C in humidified air with 5% CO_2 for 24 h. The adherent cells were treated with 10 μM and 20 μM of **R2** respectively, soluble in DMSO, for 24 h and then dropped inside the live ready probe reagent (ThermoFisher Scientific) directly for about 30 min to stain the living cell nucleus. We used a Zeiss LSM 510 META NLO DuoScan confocal microscopy equipped with a Ti:Sa multiphoton laser 690–1020 nm for two-photon excitation (TPE). **R2** (or other chemical compounds) was excited by 780 nm through TPE by a 780-nm femto-second laser to result in the corresponding excitation ultraviolet (UV) wavelength light ($\lambda_{\text{exc}} = 365$ nm) in living cells. In addition, a He–Ne laser device with excitation at 638 nm was used with the NucRed live ready probe reagent. The living cells were observed with a $\times 40$ magnification oil objective.

2.7 | Photofading behaviour of probes in living cells

MDA-MB231 cells were placed in chambered cover glass and incubated at 37°C for 24 h. Afterwards adherent cells were treated with 20 μM of **R2** in DMSO for 24 h, 48 h or 72 h. We used a Zeiss LSM 510 META NLO DuoScan confocal microscopy with an IR pulse laser source with excitation at 780 nm for chemical compounds. The living cells were observed with a $\times 40$ magnification oil objective.

3 | RESULTS AND DISCUSSION

3.1 | AIEE studies

Compounds **R1–R3** are readily soluble in dichloromethane, THF and DMSO, but insoluble in water and CH_3CN . The UV–visible absorption spectra of **R1–R3** in THF showed an intense band at 251–259 nm with a shoulder at 280–320 nm, corresponding to the $\pi\text{--}\pi^*$ transition of $\text{C}=\text{C}$ in the aromatic chromophore (Figure 1).^[59] The broad band located at 387–400 nm corresponded to $n\text{--}\pi^*$ transition of nitrogen atom promoted from their non-bonding molecular orbital to a π antibonding molecular orbital within the molecule.

The absorption spectra of **R1–R3** were recorded to check the behaviour of these compounds when different fractions of water were added into the THF solution of these compounds. The UV–vis absorption spectra of **R1–R3** (4 μM) in the presence of different percentages of water are shown in Figure 2. Upon addition of water (0–90%), absorbance was decreased in the UV region without any considerable shift in the λ_{max} value. Conversely, on the addition of 90% water, absorbance increased swiftly in the visible region (~ 500 nm), probably caused by the light scattering or Mie effect of the nanoaggregate suspensions.^[60] The results confirmed that **R1–R3** underwent aggregation to form nanoparticles in the aqueous mixture containing $\sim 80\%$ of water for both **R1** and **R2**, but 90% of water for **R3** and that the

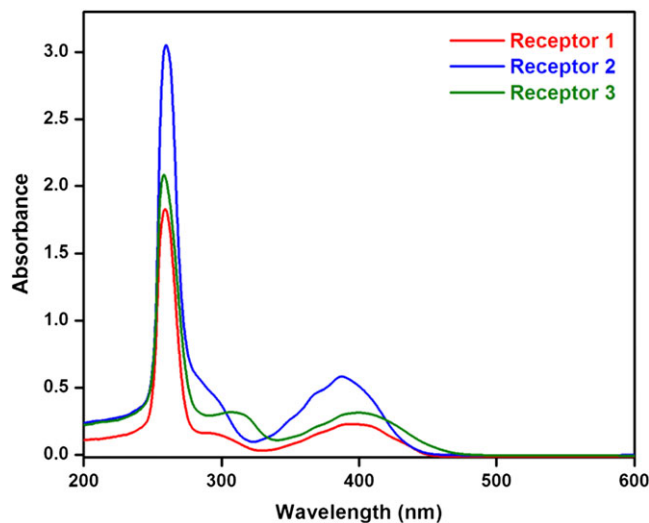


FIGURE 1 Absorption spectra of **R1–R3** (4 μM) in THF solution

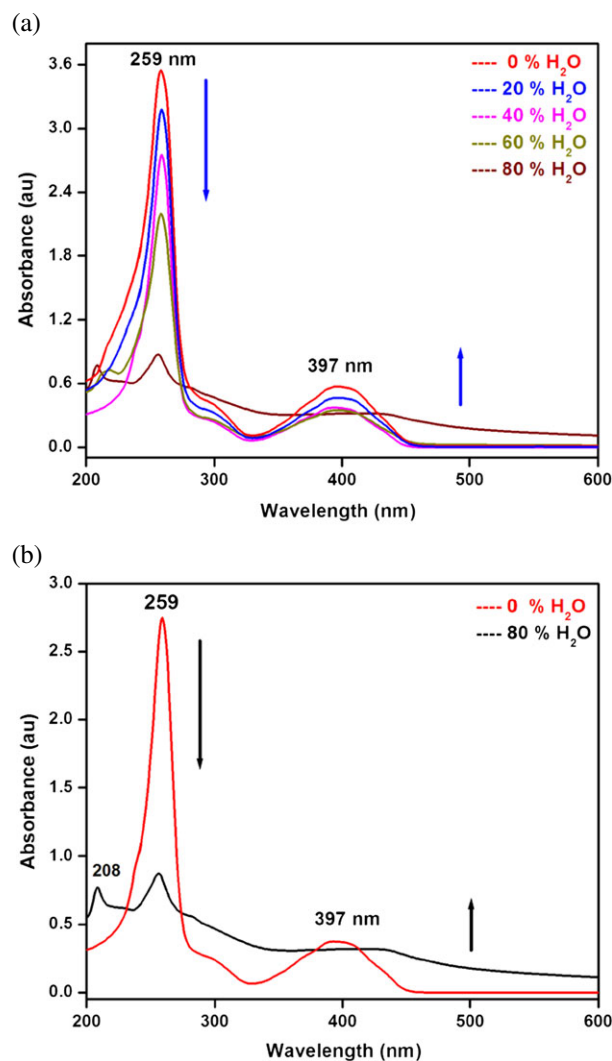


FIGURE 2 (a) UV–vis absorption spectra of **R1** in a THF/water mixture. (b) Overlay spectra of 0% H_2O and 80% H_2O

solution became slightly turbid. Levelling-off of the tail in the visible region of the absorption spectrum suggested the formation of nanoscopic aggregates of **R1–R3** (Figures S8 and S9).

The fluorescence spectra of these compounds (**R1–R3**) in THF were recorded; these three compounds exhibited weakly structured emission bands at 430–460 nm upon excitation at 400 nm (Figure S10). Interestingly, upon addition of water to the THF solution of **R1**, emission intensity was enhanced more than 10 times with a red shift of about 15 nm from 464 nm to 479 nm (Figure 3). These spectral changes indicated that a strong aggregation occurred in the emission spectra at 80% water content. Similar behaviour was also observed with **R2** and **R3**, after the successive addition of water (Figures S11 and S12). The emission quantum yield value for **R1** was increased from 0.08 to 0.15 after adding 90% water content into THF solution of **R1**.

This emission enhancement was attributed to the restriction of C=N isomerization of the anthracene rings and thus suppression of the non-radiative pathway and enhancement of fluorescence intensity.^[47] These compounds were weakly fluorescent due to isomerization of the C=N bond in the excited state. Fluorescence intensity increased drastically during aggregation due to suppression of C=N isomerization, which deactivated the non-radiative pathway in the excited state.^[61,62] The fluorescence properties of these compounds in solid-state thin films have also been investigated. Figure S13 shows the fluorescence emission of **R1–R3** in the film. All three compounds

showed an emission maximum in the range 540–565 nm, which was red-shifted by 60–115 nm compared with that of the THF/H₂O solution because of an increase in intermolecular interaction. SEM was used to investigate the formation of nanoaggregates and to examine the morphology of aggregates that formed in THF/water mixtures with high f_w (water fraction) values. SEM analysis showed that the **R1** aggregate was structurally microstones, whereas **R2** had a flower-shaped structure, both with a diameter of a few hundred nanometres. When the water fraction was increased from 80% to 90%, the **R3** structure changed from cluster-ordered microspheres to rod-shaped nanoparticles (Figure 4). Size decreased, while regularity of morphology increased concomitantly because of the high concentration of water. The difference in morphology indicated that the size and shape of the microstructures correlated with the THF/water ratio and the concentration of the solution. It is believed that in mixtures with a low water fraction the solute molecules steadily assemble in an ordered fashion to form less emissive crystalline aggregates, while in mixtures containing high water content the solute molecules quickly agglomerate in a random way to form highly emissive amorphous particles.

AFM images show that the sizes of compounds **R1–R3** were in the range 100–500 nm, confirming the formation of aggregates in the THF/H₂O mixture. AFM images of **R1–R3** in $f_w = 80\%$ H₂O for **R1** and **R2** and $f_w = 90\%$ H₂O for **R3** are shown in Figure 5. The topography of the surface showed that the aggregates were spherical and rod shaped, similar to the SEM images and matching well with previous reports.^[63]

3.2 | Sensing of BSA

In order to learn about the binding strength of compounds **R1–R3** with BSA, absorption spectral titrations were carried out in aqueous medium. The compound concentration used for the absorption spectral study was fixed at 4 μM and the BSA concentration was varied from 2 μM to 20 μM in phosphate buffer at pH = 7.4. The UV-vis absorption spectra of **R1** (4 μM) with gradual addition of BSA are shown in Figure 6.

On increasing the BSA concentration, apart from an increase in BSA absorbance at wavelengths 256 and 276 nm, a substantial change in the absorbance intensity of compounds **R1–R3** with a slight blue shift was noted. These results showed the strong binding of compounds **R1–R3** with BSA. These spectral changes clearly implied a change in the probe environment, as the probe was transferred from the aqueous phase to the protein interior. This blue shift observed in the presence of BSA prompted us to propose binding of the protein with these compounds through hydrogen bonding as well as via hydrophobic interactions, and also supported by theoretical studies. The same trend in absorption has been observed in spectral studies with other compounds (Figures S14 and S15). Although BSA showed no absorption at 300–400 nm, addition of BSA led to a substantial increase in absorbance at these wavelengths and these spectral changes were used to calculate the binding constant (K) using equation 1^[64]

$$\frac{A_0}{A-A_0} = \frac{\epsilon_{BSA}}{\epsilon_c} + \left(\frac{\epsilon_{BSA}}{\epsilon_c \cdot K_b} \right) \times \frac{1}{[BSA]} \quad (1)$$

Here, A_0 and A are the absorbance of compounds **R1–R3** at 257 nm in the absence or presence of BSA. ϵ_v and ϵ_c are the molar

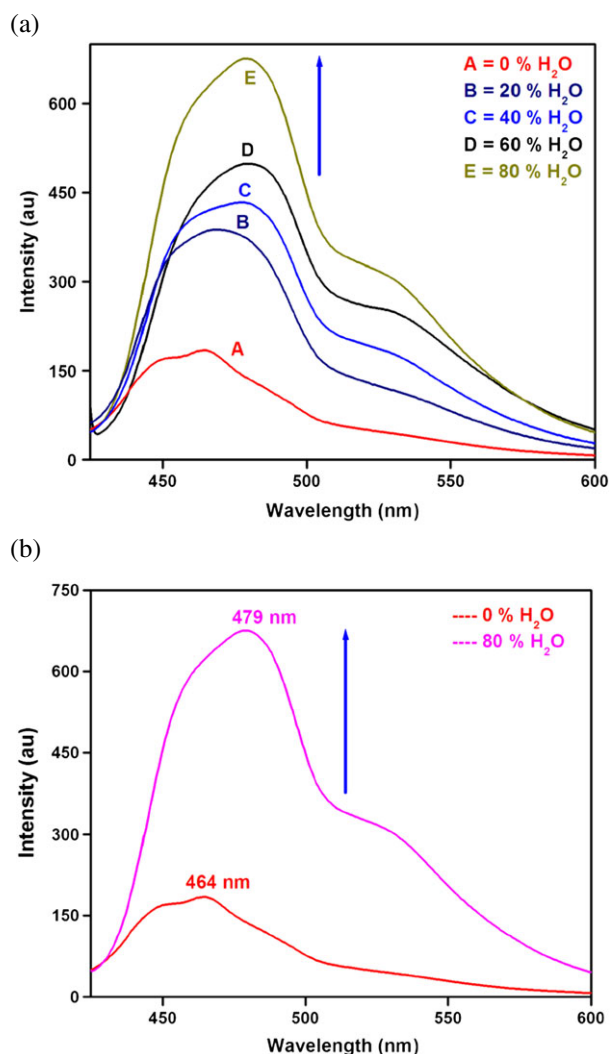


FIGURE 3 (a) Emission spectra of **R1** (4 μM) in THF/water mixture. (b) Overlay spectra of 0% and 80% H₂O

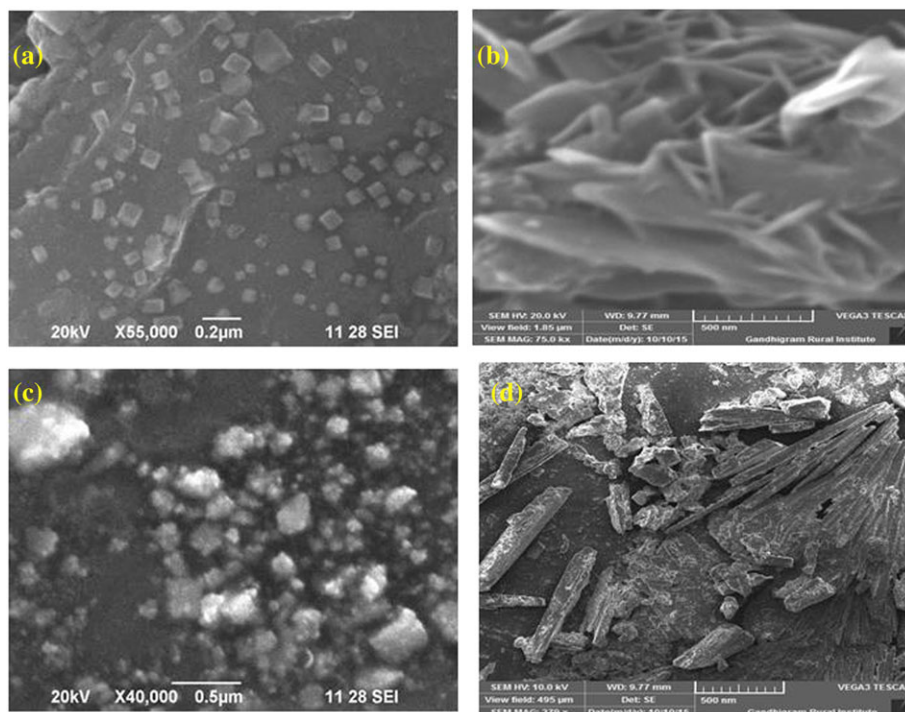


FIGURE 4 (a) SEM images of (a) R1 (THF:H₂O, 80%:20%, v/v); (b) R2 (THF:H₂O, 80%:20%, v/v); (c) R3 (THF:H₂O, 80%:20%, v/v); and (d) R3 (THF:H₂O, 90%:10%, v/v)

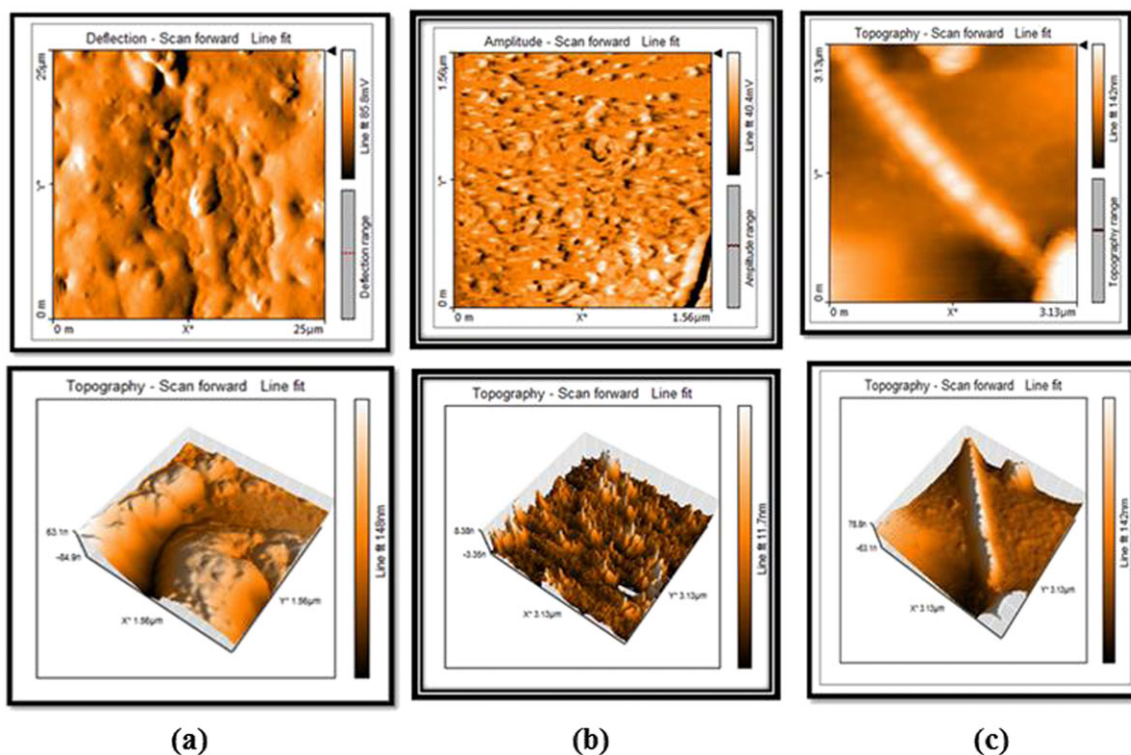


FIGURE 5 Atomic force microscopy (AFM) images of (a) R1 (THF:H₂O, 80%:20%, v/v); (b) R2 (THF:H₂O, 80%:20%, v/v); and (c) R3 (THF:H₂O, 90%:10%, v/v)

extinction coefficients of free and BSA bound compounds, respectively. Therefore, the binding constant (K_b) was estimated from the ratio of the intercept to the slope in the linear double reciprocal plot of $1/(A - A_0)$ versus $1/[BSA]$. The binding constant values for the

binding of these compounds with BSA calculated from the UV-vis absorption spectral data are given in the Table 1.

To confirm the interaction between compounds R1–R3 and proteins, a fluorescence titration was carried out keeping the R1–R3

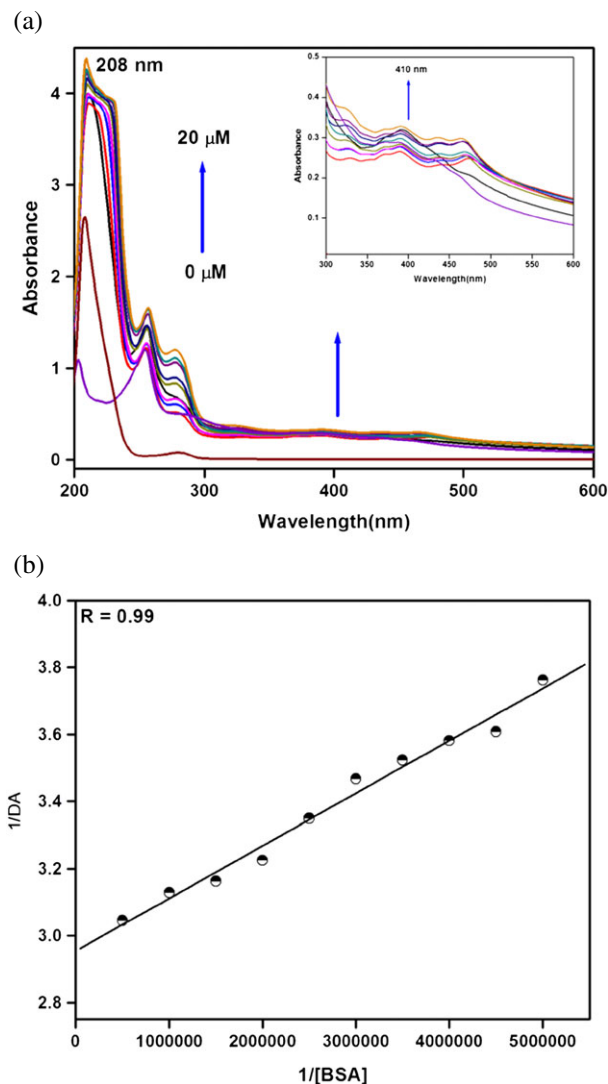


FIGURE 6 (a) UV-visible absorption spectral changes during titration of **R1** with BSA. Inset shows the spectral changes at 350 nm. (b) Double reciprocal plot of **R1** with BSA

concentration constant while varying the BSA concentration (Figures 7, S16 and S17).

The emission intensity of **R1–R3** was found to be enhanced gradually on increasing the BSA concentration because changes in the secondary/tertiary structure of proteins in phosphate buffer medium affected the orientation of amino acid residues in the protein. The enhancement of emission intensity was due to the strong binding of **R1–R3** with BSA through hydrophobic interactions, and the rigidity of their local surroundings upon binding to the protein.^[65] Another possibility was that protein bound with **R1–R3** through hydrogen bonding, which also led to emission enhancement due to

TABLE 1 Binding constant values for compounds (**R1–R3**) with BSA

Compounds	Binding constant K_b , M^{-1}	
	Absorption	Emission
R1	1.8×10^5	1.7×10^5
R2	5.4×10^7	3.9×10^7
R3	6.0×10^6	2.6×10^6

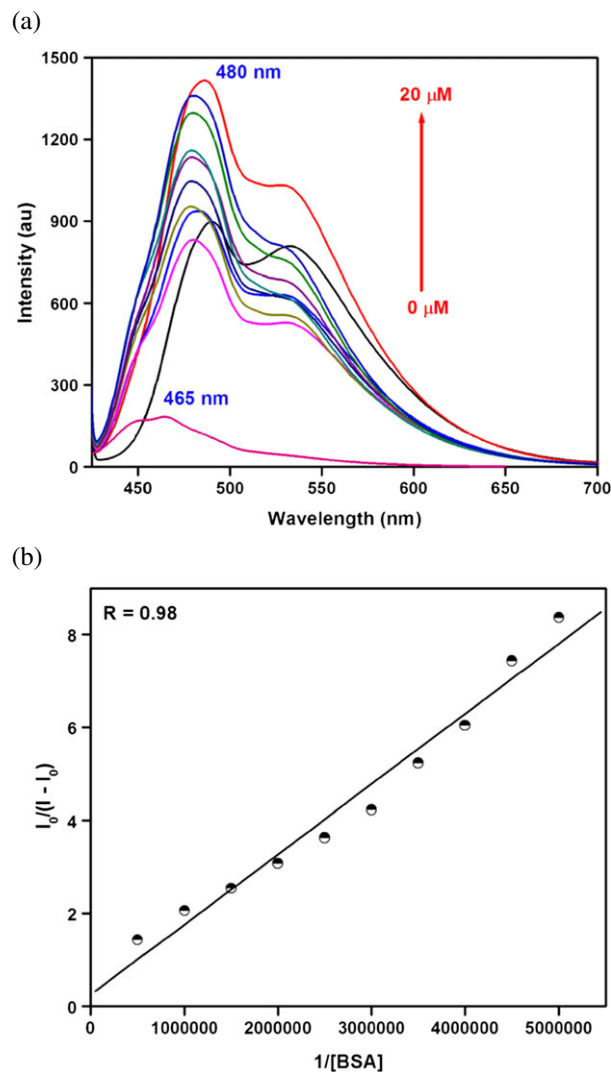


FIGURE 7 (a) Fluorescence emission spectral changes of compound **R1** during the titration with BSA. (b) Plot for the calculation of binding constant for the binding of **R1** with BSA

favourable thermodynamic parameters.^[66,67] Therefore, it was proposed that the combined effect of hydrogen bonding along with hydrophobic interaction was responsible for this emission enhancement. The binding constants were calculated using the modified Benesi–Hildebrand equation (equation 2) and these values are also given in Table 1.^[68]

$$\frac{I_0}{I - I_0} = \frac{b}{(a-b)} \left(\frac{1}{K_b[BSA] + 1} \right) \quad (2)$$

where I and I_0 are the luminescence intensities of the compounds in the presence or absence of BSA, respectively. K_b is the binding constant, 'a' and 'b' are constants. It is interesting to note that the binding constant values estimated by UV-visible absorption and emission spectral studies were in good agreement. This binding constant value was quite high compared with other reports.^[69,70] Molecular docking studies also reveal the strong interaction between compounds **R1–R3** and BSA (Figure 8). For the docking studies, the crystal (3D) structure of BSA was downloaded from the Protein Data Bank. Figure 8 shows that compound **R2** is surrounded by BSA residues

(LYS20, GLU17, LYS41, LYS131, GLU48, ASN44). Among the surrounded residues, compound **R2** interacts with the LYS20 residue and is stabilized via hydrogen bonding between the oxygen atom of **R2** and lysozyme amine group with a bond distance of 2.6 Å. It is clearly evident that the interaction between protein and probes occurred through the hydrophobic cavity of proteins via hydrogen bonding.

3.3 | Cell toxicity of probes

In order to apply anthracene as a fluorescent probe in living cells, the minimum cytotoxic requirement is crucial for empirical development and to establish suitable protocols for different cells. Therefore, the cytotoxicity of these probes (**R2**) at different concentrations from 10 to 50 µM on human breast cancer cells (BT-549 and MDA-MB-231) over a period of 24 h was evaluated using MTT assays (Figure 9). Interestingly, **R2** displayed less toxicity (up to 50 µM) to MDA-MB-231 cells under the experimental conditions. Therefore, **R2** exhibited low cytotoxicity, with cell viabilities >70% at concentrations up to 20 µM, suggesting that **R2** is a biocompatible probe and may have potential application in live-cell imaging.

3.4 | Fluorescence imaging of living cells

To validate the potential applications of **R2** in live-cell imaging, we first conducted preliminary cell microscopy experiments using both BT549 and MDA-MB231 cell lines to check whether these probes have a fluorescent signal in living cell using a fluorescence microscope to give a corresponding excitation of UV wavelength light (about $\lambda_{exc} = 365$ nm) in living cells. As shown in Figure S17, **R2** (10 µM and 20 µM) in living cells (BT549) was easily excited through TPE by a 780-nm femtosecond laser and displayed blue emission collected from the blue channel ($\lambda_{em} = 450$ nm). In contrast, cells stained with **R1** and **R3** emitted no or a weak intracellular fluorescence signal (blue) (Figure S18). These experiments suggested that the rapid internalization of the **R2** probe by cells would allow imaging studies with live cells. Therefore, we evaluated the applicability of **R2** for its ability to penetrate cell membranes and its molecular mode of action in live-cell imaging using confocal laser scanning microscopy.

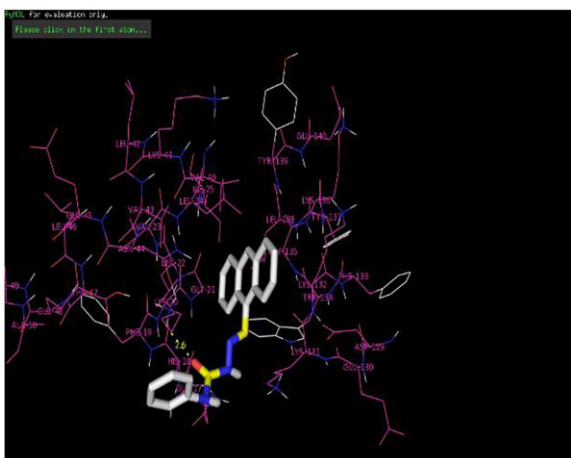


FIGURE 8 Different docking images of compound **R2** with BSA

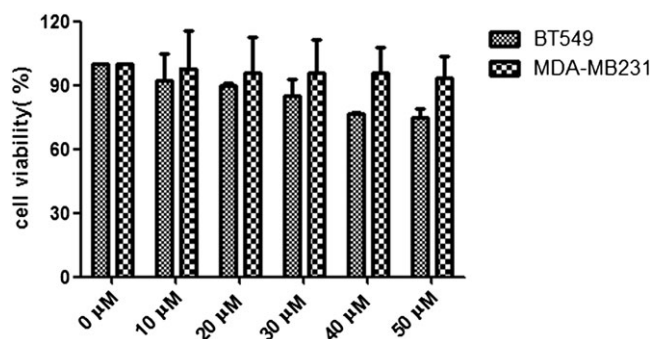


FIGURE 9 The cytotoxicity of fluorescent compound **R2** for BT549 and MDA-MB231 over 24 h

In control experiments with live BT549 cells, red fluorescence indicated that the cells were stained by NucRed, a live ready probe reagent (NucRed®, red staining), the nucleus marker (Figure S18) and consecutively excited through a He-Ne laser with excitation at 638 nm. Representative fluorescence images of live cells were treated with 10 µM of **R2**, respectively, on 8-well plates for 24 h and subsequently stained by NucRed® (red, a cell-permeant nuclear stain) after 30 min of incubation (Figure S18b, c). As shown in Figure S17, the BT549 cells incubated with these probes displayed intracellular fluorescence emission (blue) in a dose-dependent manner, indicating direct visualization of **R2** internalized by cells. The cell images showed that the probe could homogeneously localize in the cytoplasm, and could be differentiated from the presence of a NucRed® nuclear localization signal. Similarly, MDA-MB231 cells stained by 10 µM or 20 µM **R2** emitted blue fluorescence emission in a dose-dependent manner (Figure S19b, c) compared with the control NucRed® probe (Figure S19).

In this section, we have further identified the **R2** compound, which possesses a core structure of an anthracene-based Schiff base complex, as a cell-permeant dye for live-cell imaging, discovering the workable excitation wavelength of 780 nm through TPE using a femtosecond laser. It should be noted that TPE with an infra-red laser rather than single photon excitation is known to demonstrate both less collateral damage to normal cell/tissue and better cell/tissue penetration ability. Taken together, the results suggested that **R2** is internalized by human breast cancer cell lines and verified their potential as

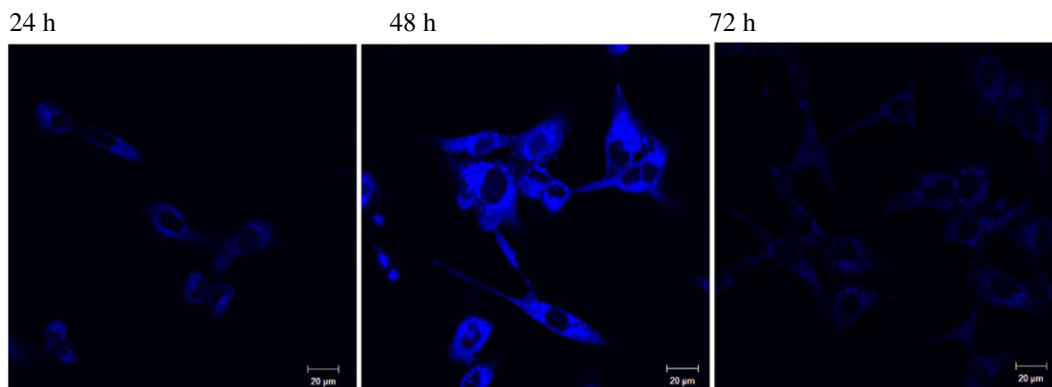


FIGURE 10 Living MDA-MB231 cells were treated with 20 μM of **R2** for 24, 48, or 72 h. The cells were observed under a Zeiss confocal microscope and experimental conditions were the same as described above. Scale bar = 20 μm

fluorescent dyes through cell imaging with live-cell fluorescence microscopy.

3.5 | Long-term cell imaging using R2 probe

Development of cell-staining fluorophores has gained unexpected attention because these materials have been widely used in live-cell imaging, biological quantification, and medical diagnosis.^[71] However, they frequently suffer from the problems of photostability, light-fastness, toxicity and photobleaching during laser scanning that retard their further applications as biocompatible fluorophores in living cells.^[72] To gain insights into long-term cell imaging using the **R2** probe in live-cell imaging, the imaging performance of this probe was investigated over different time periods, 24, 48, or 72 h using confocal laser scanning microscopy (Figure 10). The intensity of fluorescence in MDA-MB231 cells increased with time up to 48 h and gradually decayed at 72 h. Interestingly, the analysis of living cells implied that uptake of the **R2** probe occurred mostly at 48 h of incubation and this action provided urgently needed information for the long-term observation of live cells up to 72 h. The findings indicated that the **R2** probe is a considerable and stable fluorophore, suggesting that this low cytotoxicity probe may be a potential candidate as a fluorescence tool for exposing targets and dynamic mechanisms of action in live cells.

4 | CONCLUSION

In summary, we have designed three anthracene-based receptors comprised of amide, urea and thiourea moieties with AIEE characteristics, which served as excellent fluorescent probes for BSA and optical cell imaging for cancer cells. In THF, these compounds were weakly emissive but after addition of 90% water the emission intensity was enhanced, due to the AIEE effect and nanoaggregate formation confirmed by microscopic techniques. These compounds bound efficiently with BSA with a binding constant in the order 10^5 – 10^7 M^{-1} leading to emission enhancement. These probes showed less toxicity towards human breast cancer cell lines and their potential as fluorescent dyes through live-cell fluorescence microscopy. Further research is expected on these molecules to detect metal ions and anions in biological as well as environmental samples.

ACKNOWLEDGEMENTS

S.R. wishes to thank UGC, New Delhi for a UGC-BSR Faculty Fellowship and Emeritus Fellowship. A.M acknowledges UGC for FDP and VOC College management, Tuticorin for providing facility. V.S is the recipient of a SERB-Indo US postdoctoral research fellowship. We are also grateful for financial support of this work provided by the Academia Sinica and the National Science Council (NSC 102-2325-B-001-025 and MOST 103-2113-M-001-024-MY3). Instrument support was provided by the Chemical Biology Facility in the Institute of Chemistry at Academia Sinica, Taiwan. Experiments and data analysis were performed in part through the use of the confocal microscope at the Division of Instrument Service of Academia Sinica and with the assistance of Shu-Chen Shen.

FUNDING INFORMATION

UGC-BSR Faculty Fellowship and Emeritus Fellowship. SERB-Indo US postdoctoral research fellowship. Academia Sinica and the National Science Council (NSC 102-2325-B-001-025 and MOST 103-2113-M-001-024-MY3).

ORCID

Arumugam Ramdass  <http://orcid.org/0000-0001-6108-121X>

Veerasamy Sathish  <http://orcid.org/0000-0002-7097-4658>

Pounraj Thanasekaran  <http://orcid.org/0000-0001-6437-7366>

REFERENCES

- [1] R. Furue, T. Nishimoto, I. S. Park, J. Lee, T. Yasuda, *Angew. Chem. Int. Ed.* **2016**, *55*, 7171.
- [2] A. Kitai, *Luminescent Materials and Applications*, John Wiley Sons **2008**.
- [3] R. B. Thompson, *Fluorescence Sensors and Biosensors*, CRC, Boca Raton **2006**.
- [4] T. D. Ashton, K. A. Jolliffe, F. M. Pfeffer, *Chem. Soc. Rev.* **2015**, *44*, 4547.
- [5] J. B. Birks, *Photophysics of Aromatic Molecules*, Wiley, London **1970**.
- [6] Z. Zhelev, H. Ohba, R. Bakalova, *J. Am. Chem. Soc.* **2006**, *128*, 6324.
- [7] J. Luo, Z. Xie, J. W. Y. Lam, L. Cheng, H. Chen, C. Qiu, H. S. Kwok, X. Zhan, Y. Liu, D. Zhu, B. Z. Tang, *Chem. Commun.* **2001**, 1740.
- [8] B. Z. Tang, X. Zhan, G. Yu, P. P. S. Lee, Y. Liu, D. Zhu, *J. Mater. Chem.* **2001**, *11*, 2974.
- [9] A. Qin, B. Z. Tang, *Aggregation-Induced Emission: Principles, Aggregation Induced Emission: Applications, Vols I and II*, John Wiley and Sons **2013**.

- [10] S. Kumar, P. Singh, A. Mahajan, S. Kumar, *Org. Lett.* **2013**, *15*, 3400.
- [11] Y. Hong, J. W. Y. Lam, B. Z. Tang, *Chem. Soc. Rev.* **2011**, *40*, 5361.
- [12] R. Hu, N. L. Leung, B. Z. Tang, *Chem. Soc. Rev.* **2014**, *43*, 4494.
- [13] J. Mei, N. L. C. Leung, R. T. K. Kwok, J. W. Y. Lam, B. Z. Tang, *Chem. Rev.* **2015**, *115*, 11718.
- [14] B. Manimaran, P. Thanasekaran, T. Rajendran, R. J. Lin, I. J. Chang, G. H. Lee, S. M. Peng, S. Rajagopal, K.-L. Lu, *Inorg. Chem.* **2002**, *41*, 5323.
- [15] V. Sathish, A. Ramdass, P. Thanasekaran, K.-L. Lu, S. Rajagopal, *J. Photochem. Photobiol. C: Rev.* **2015**, *23*, 25.
- [16] Z. Zhao, B. Hea, B. Z. Tang, *Chem. Sci.* **2015**, *6*, 5347.
- [17] Z. Zhao, J. W. Y. Lam, B. Z. Tang, *J. Mater. Chem.* **2012**, *22*, 23726.
- [18] V. Mahendran, K. Pasumpon, S. Thimmarayaperumal, P. Thilagar, S. Sivakumar, *J. Org. Chem.* **2016**, *81*, 3597.
- [19] M. Boominathan, V. Sathish, M. Nagaraj, N. Bhuvanesh, S. Muthusubramanian, S. Rajagopal, *RSC Adv.* **2013**, *3*, 22246.
- [20] Z. Yu, Y. Duan, L. Cheng, Z. Han, Z. Zheng, H. Zhou, J. Wu, Y. J. Tian, *J. Mater. Chem.* **2012**, *22*, 16927.
- [21] B.-K. An, J. Gierschner, S. Y. Park, *Acc. Chem. Res.* **2012**, *45*, 544.
- [22] B. K. An, S. K. Kwon, S. D. Jung, S. Y. Park, *J. Am. Chem. Soc.* **2002**, *124*, 14410.
- [23] B. K. An, D. S. Lee, Y. S. Park, H. S. Song, S. Y. Park, *J. Am. Chem. Soc.* **2004**, *126*, 10232.
- [24] I. Manikandan, C. H. Chang, C. L. Chen, V. Sathish, W. S. Li, M. Malathi, *Spec. Chim. Acta Part A* **2017**, *58*, 182.
- [25] V. Mukundam, A. Kumar, K. Dhanunayarao, A. Ravi, S. Peruncheralathan, K. Venkatasubbaiah, *Polym. Chem.* **2015**, *6*, 7764.
- [26] S. Mukherjee, P. S. Salini, A. Srinivasan, S. Peruncheralathan, *Chem. Commun.* **2015**, *51*, 17148.
- [27] K. K. Neena, P. Thilagar, *J. Mater. Chem. C* **2016**, *4*, 11465.
- [28] G. R. Kumar, S. K. Sarkar, P. Thilagar, *Chem. A Eur. J.* **2016**, *22*, 1.
- [29] Y. Hong, L. Meng, S. Chen, C. W. T. Leung, L. T. Da, M. Faisal, D. A. Silva, J. Liu, J. W. Y. Lam, X. Huang, B. Z. Tang, *J. Am. Chem. Soc.* **2012**, *134*, 1680.
- [30] Z. Wang, L. Yan, L. Zhang, Y. Chen, H. Li, J. Zhang, Y. Zhang, X. Li, B. Xu, X. Fu, Z. Sun, W. Tian, *Polym. Chem.* **2014**, *5*, 7013.
- [31] H. Shi, J. Liu, J. Geng, B. Z. Tang, B. J. Liu, *J. Am. Chem. Soc.* **2012**, *134*, 9569.
- [32] A. Kathiravan, K. Sundaravel, M. Jacco, G. Dhinakaran, A. Rameshkumar, D. Arul Ananth, T. Sivasudha, *J. Phys. Chem. B* **2014**, *118*, 13573.
- [33] S. Choi, J. Bouffard, Y. Kim, *Chem. Sci.* **2014**, *5*, 751.
- [34] J. Zhang, B. Xu, J. Chen, L. Wang, W. Tian, *J. Phys. Chem. C* **2013**, *117*, 23117.
- [35] V. Sathish, A. Ramdass, Z.-Z. Lu, M. Velayudham, P. Thanasekaran, K.-L. Lu, S. Rajagopal, *J. Phys. Chem. B* **2013**, *117*, 14358.
- [36] J. Wang, J. Mei, R. Hu, J. Z. Sun, A. Qin, B. Z. Tang, *J. Am. Chem. Soc.* **2012**, *134*, 9956.
- [37] N. Zhao, Y.-H. Wu, J. Luo, L.-X. Shi, Z.-N. Chen, *Analyst* **2013**, *138*, 894.
- [38] Y. Q. Sun, P. Wang, J. Liu, J. Zhang, W. Guo, *Analyst* **2012**, *137*, 3430.
- [39] T. J. Peters, *All About Albumin Biochemistry, Genetics, and Medical Applications*, Academic Press, San Diego, CA **1996**.
- [40] J. S. Mandeville, H. A. Tajmir-Riahi, *Biomacromolecules* **2010**, *11*, 465.
- [41] X. M. He, D. C. Carter, *Nature* **1992**, *358*, 209.
- [42] C. V. Kumar, A. Buranaprapuk, G. J. Opiteck, M. B. Moyer, S. Jockusch, N. J. Turro, *Proc. Natl. Acad. Sci. U. S. A.* **1998**, *95*, 10361.
- [43] S. Naveenraj, S. Anandan, *J. Photochem. Photobiol. C: Photochem. Rev.* **2013**, *14*, 53.
- [44] C. A. Terry, M.-J. Fernandez, L. Gude, A. Lorente, K. B. Grant, *Biochemistry* **2011**, *50*, 10375.
- [45] F. A. Holmes, L. Esparza, H. Y. Yap, A. U. Buzdar, G. R. Blumenschein, G. N. Hortobagyi, *Cancer Chemother. Pharmacol.* **1986**, *18*, 157.
- [46] B. S. Iyengar, R. T. Dorr, D. S. Alberts, A. M. Sólyom, M. Krutzsch, W. A. Remers, *J. Med. Chem.* **1997**, *40*, 3734.
- [47] K. Namitharan, K. Pitchumani, *Org. Biomol. Chem.* **2012**, *10*, 2937.
- [48] A. Ramdass, V. Sathish, M. Velayudham, P. Thanasekaran, K.-L. Lu, S. Rajagopal, *Inorg. Chem. Commun.* **2013**, *35*, 186.
- [49] V. Srinivasan, M. A. Jhonsi, N. Dhenadhayalan, K. C. Lin, M. Jaccob, A. Kathiravan, *Chem. Select* **2017**, *2*, 1353.
- [50] S. Xue, X. Qiu, Q. Sun, W. Yang, *J. Mater. Chem. C* **2016**, *4*, 1568.
- [51] L. Bu, M. Sun, D. Zhang, W. Liu, Y. Wang, M. Zheng, S. Xue, W. Yang, *J. Mater. Chem. C* **2013**, *1*, 2028.
- [52] Y. Wang, W. Liu, L. Bu, J. Li, M. Zheng, D. Zhang, M. Sun, Y. Tao, S. Xue, W. Yang, *J. Mater. Chem. C* **2013**, *1*, 856.
- [53] W. Liu, Y. Wang, M. Sun, D. Zhang, M. Zheng, W. Yang, *Chem. Commun.* **2013**, *49*, 6042.
- [54] Y. Wang, T. Liu, L. Bu, J. Li, C. Yang, X. Li, Y. Tao, W. Yang, *J. Phys. Chem. C* **2012**, *116*, 15576.
- [55] W. Liu, Y. Wang, L. Bu, J. Li, M. Sun, D. Zhang, M. Zheng, C. Yang, S. Xue, W. Yang, *J. Luminesc* **2013**, *143*, 50.
- [56] J. Dong, W. Liu, S. Ying, Y. Wu, S. Xue, W. Yang, *J. Luminesc* **2016**, *176*, 168.
- [57] J. Chan, S. C. Dodani, C. J. Chang, *Nat. Chem.* **2012**, *4*, 973.
- [58] G. A. Crosby, J. N. Demas, *J. Phys. Chem.* **1971**, *75*, 991.
- [59] N. Turro, V. Ramamurthy, J. C. Scaiano, *Modern Molecular Photochemistry of Organic Molecules*, University Science **2010**.
- [60] B. Z. Tang, Y. Geng, J. W. Y. Lam, B. Li, X. Jing, X. Wang, F. Wang, A. B. Pakhomov, *Chem. Mater.* **1999**, *11*, 1581.
- [61] J. S. Wu, W. M. Liu, J. C. Ge, H. Y. Zhang, P. F. Wang, *Chem. Soc. Rev.* **2011**, *40*, 3483.
- [62] A. Ramdass, V. Sathish, M. Velayudham, P. Thanasekaran, S. Umopathy, S. Rajagopal, *RSC Adv.* **2015**, *5*, 38479.
- [63] X. Wang, Y. Yang, D. Wu, Y. Zhuang, P. Gao, F. Yang, H. Shen, H. Guo, *Biomacromolecules* **2016**, *17*, 2920.
- [64] K. A. Connors, *Binding Constants*, John Wiley & Sons, USA **1987**.
- [65] V. Sathish, A. Ramdass, E. Babu, Z.-Z. Lu, T. T. Chang, M. Velayudham, P. Thanasekaran, K.-L. Lu, W. S. Li, S. Rajagopal, *RSC Adv.* **2013**, *3*, 18557.
- [66] X. Yu, Z. Liao, B. Jiang, X. Hua, X. Lia, *Spectrochim. Acta A* **2015**, *137*, 129.
- [67] R. Wang, H. Dou, Y. Yin, Y. Xie, L. Sun, C. Liu, J. Dong, G. Huang, Y. Zhu, C. Song, J. Chang, *J. Luminesc* **2014**, *154*, 8.
- [68] S. P. Upadhyay, R. R. S. Pissurlenkar, E. C. Coutinho, A. V. Karnik, *J. Org. Chem.* **2007**, *72*, 5709.
- [69] B. Ohja, G. Das, *Photochem. Photobiol. Sci.* **2011**, *10*, 554.
- [70] J. Wang, H.-B. Liu, S. Park, S. Y. Kim, T. Joo, C.-S. Ha, *RSC Adv.* **2012**, *2*, 4242.
- [71] W. E. Briley, M. H. Bondy, P. S. Randeria, T. J. Dupper, C. A. Mirkin, *Proc. Natl. Acad. Sci. U. S. A.* **2015**, *112*, 9591.
- [72] M. Bruchez Jr., M. Moronne, P. Gin, S. Weiss, A. P. Alivisatos, *Science* **1998**, *281*, 2013.

SUPPORTING INFORMATION

Additional Supporting Information may be found online in the supporting information tab for this article.

How to cite this article: Densil S, Chang C-H, Chen C-L, et al. Aggregation-induced emission enhancement of anthracene-derived Schiff base compounds and their application as a sensor for bovine serum albumin and optical cell imaging. *Luminescence*. 2018;1–10. <https://doi.org/10.1002/bio.3477>